Journal of Applied Electrochemistry (2005) 35:17–26
DOI 10.1007/s10800-004-2054-9

Anomalous electrical conductivity of aqueous solutions in submicron cracks and gaps

VICTOR A. MARICHEV
Department of Chemistry, University of Western Ontario, London, Ontario, Canada N6A 5B7 e-mail:vmariche@uwo.ca; marichev@rogers.com

Received 08 September 2003; accepted 16 July 2004

Key words: conductivity, contact electrical resistance, hydrogen bond network, stress corrosion cracking, submicron cracks

Abstract

By a modified technique of contact electrical resistance (CER), the electrical conductivity of alcohol and aqueous solutions of acids, salts, and bases in submicron gaps between clean contact surfaces have been measured. Alcohol solutions of water content below 10% do not have substantial electrical conductivity, while at contents of about 50% their electrical conductivity becomes similar to that of aqueous solutions. The electrical conductivity of dilute aqueous solutions is anomalously high. It is higher than that of strong solutions of salts and acids, in contradiction with the ionic theory of electrical conductivity. A conclusion on the nonionic nature of the electrical conductivity of aqueous solutions in submicron gaps is formulated. A model of electrical conductivity assuming the formation of a labile spatial hydrogen-bond network in the contact gap is proposed and used to explain the results.

1. Introduction

The spatial distribution of electrochemical and corrosion processes in narrow long tubes, slits, cracks, and other defects has been studied theoretically since 1970. Equations obtained allow estimation of the function of porous electrodes and the possibility of electrochemical protection against pitting corrosion and stress corrosion cracking (SCC). A short review of early investigations was given by Frumkin [1] who introduced the concept of the critical parameter L_{cr}:

$$L_{cr} = N(W/\rho K)^{0.5}, \quad (1)$$

where N is a dimensionless constant determined by the geometry of a defect, W is its thickness or radius, ρ is the resistivity of an electrolyte inside the defect, and K is a constant which depends on the polarization characteristics of the defect walls. The L_{cr} value ($L_{cr}/W^{0.5}$ or L_{cr}^2/W in later work [2–4]) determines the distribution of current and potential E_L along the defect depending on the polarization potential E_0.

A change in the polarization current and E_L inside a defect should be most pronounced at a distance of L_{cr} from the polarization source [1]. The narrower the crack, or the higher the resistivity of an electrolyte in it, the smaller this distance. For cathodic protection of a growing corrosion fatigue crack, with $W = 4$ μm and $E_0 \to \infty$ (i.e., at an infinite power of the external polarization source), the limiting E_L value tends to zero for a depth of crack $L = 50$ μm, i.e., $L_{cr} = 12$ W [2]. A similar value ($L_{cr} = 15$ W) was obtained earlier [1]. When the nuclear power industry began to rapidly develop and it was realized that SCC could be a cause of accidents, corrosion in cracks became a subject of keen interest [3–6].

Much experimental data on the polarization of specimens with submicron cracks and gaps cannot be described in terms of the L_{cr} concept [1–6], especially with regard to SCC of high-strength materials [7–9] and that obtained using the contact electric resistance (CER) of metals in electrolytes [10, 11]. During SCC of high-strength steels (the strength limit of 190–250 kg mm^{-2}), the external polarization substantially affects the growth of very long cracks in specimens with a thickness of 3 mm. This would be impossible if the polarization potential, controlled at the surface of a specimen, did not change the potential at the crack tip in the center of a specimen, where the tri-axial stressed state is the most pronounced. In this case $L_{cr} = 1$ mm $\approx (0.5–1)\times10^4$ W. This estimate exceeds the aforementioned values of $L_{cr} = (12–15)$ W [1, 2] by three orders of magnitude and cannot be explained without new concepts on the conductivity of aqueous solutions in submicron cracks. In this work, the CER technique [10, 11] modified to provide estimates of the specific electric resistance of a submicron electrolyte interlayer between two working electrodes, was used.

2. Experimental

The CER technique is based on the precise measurement of the contact electric resistance between two identical

specimens periodically brought in contact in an electrolyte. As described in [9–11], the potential dependence of the CER is determined by changes due to adsorption and the presence of oxide and other films on an electrode surface and, to date, has not been used to measure the conductivity of a solution. The specimens with a 2-mm diameter were fastened in a special rigid-spring holder that prevented their lateral motion and promoted a continuous coaxial oscillation with amplitude of 5 μm $\pm$ 1 nm and a frequency of 0.2 Hz during the experiment.

Figure 1 shows a circuit for measuring the CER of two identical specimens (1) fastened with insulating holders, and placed in an electrochemical cell (2). The specimens are shunted with a resistor R_2 (0.01–10) mΩ and connected to a P5727 potentiostat (3), a B5-43 stabilized direct current source (4), and a P3009 double bridge (5). The disbalance signal of the bridge is sent to a F136/1 amplifier (6) and continuously recorded using a KSP4 recorder or a computer (7). The specimens are coaxially fastened in a rigid spring of special design (Figure 2) that prevents their side displacement. One specimen is fixed, while the other oscillates along their common axis. CER values are measured at a direct current of 0.1–1 A passing through the specimens and a resistor, R_2, connected in parallel. On each cycle, the working surfaces of the specimens are brought in contact. The amplitude of oscillations and the geometrical dimensions of the contact are maintained constant throughout the experiment, which provides high stability in CER. The CER (R) estimates are given in [9–11].

Figure 2 shows schematic of the CER device assembling on a hard plate 1 (autoclave head). A step engine 3, fastened at the stands 2 on this plate, controls the reciprocating motion of a bar 4 inserted in the autoclave through a seal 5. Inside the autoclave, a rigid spring 7 is fastened to a stand 6. The design of this spring parallelogram prevents any lateral motion of the upper mobile specimen. All components are made of a stainless steel. Teflon insulating casings for the mobile 8 and fixed 9 specimens, connected to the measuring circuit (Figure 1) with insulated wires 10, are fastened in the spring 7. This spring was loaded with a bar 4 via a

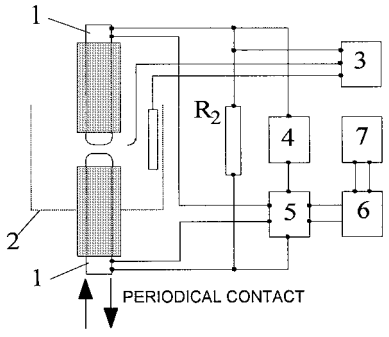

Fig. 1. The principal circuit for measuring the contact electrical resistance (CER): (1) specimens; (2) electrochemical cell; (3) potentiostat; (4) direct current source; (5) double bridge; (6) amplifier; and (7) self-recorder.

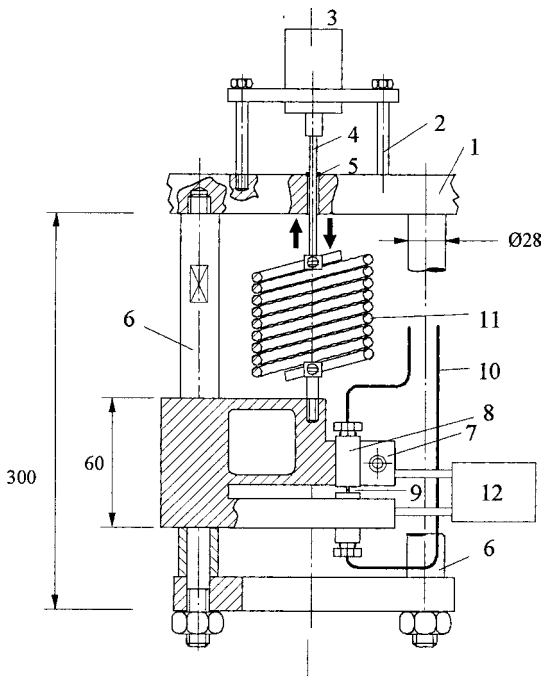

Fig. 2. The principal scheme of a device for measuring CER (see text for details).

mild spiral spring 11, the compliance of which ($C = 5$ μm kg^{-1}) is a thousand times larger than that of the rigid spring 7. This means that a shift in bar 4 and deformation of the mild spring 11 by 1 mm causes the deformation of spring 7 by only 1 μm.

The device shown in Figure 2 was immersed in the autoclave, and the spring 7 was loaded using the step engine 3 controlled by a computer [11]. In this work we used a similar device modified as follows: a small electrochemical cell was fastened directly to the holder of the lower fixed specimen, and computer control was replaced with a simple mechanical system providing the same accuracy and stability. The mild and rigid springs were loaded sinusoidally with

$$P = P_0 + P_1\sin(\omega t); \quad L = L_0 + L_1\sin(\omega t);$$
$$l = l_0 + l_1\sin(\omega t); \quad 2l_1 = A, \tag{2}$$

where P is the loading; L is the corresponding elongation of the mild spring; $l = 0.001\ L$ is the elongation of the rigid spring (a change in the distance between specimens without contact between them); A is the amplitude of the oscillations of the mobile specimen measured with a strain-gauge transducer 12 (sensitivity of 0.02 μm). When the surface properties of metals are studied [10], the A, P_0, P_1, L_0, L_1, l_0, and l_1 values are typically maintained constant for the whole series of experiments. In contrast, when measuring the conductivity of a thin electrolyte layer between the contact surfaces of the specimens, P_1 remains constant while P_0 is changed in steps within the same experimental series. This causes changes in the contact clamping.

The specimens of copper, silver, gold, and platinum (99.98 wt %) were soldered in copper holders. The area

of specimens immersed in the electrolyte was 0.2 cm^2, while their contact area was about 0.02 cm^2. The contact surfaces were sandpapered and washed in distilled water. Before each experiment, they were cleaned by cathodic polarization in the working solution. The experiments were carried out at a room temperature of 22–24 °C. In the same series of tests, the temperature variation was within 0.5 °C. The electrolyte was not deaerated, and the volume of the electrochemical cell was 5 ml. An auxiliary electrode, a platinum wire with a diameter of 0.5 and a length of 50 mm, was arranged around the specimens. The solutions were prepared from distilled water and chemically pure substances. The CER measurements were carried out under potentiostatic or galvanostatic polarization. All potential values below are quoted against the normal hydrogen electrode (NHE).

3. Results and discussion

3.1. *Reduction and oxidation of the clamped contact surfaces*

Each series of experiments was started with cathodic cleaning of the specimens in the working solution [9–11]. CER measurements on the kinetics of submonolayer oxidation of copper and silver were described in [10] where an interesting and paradoxical regularity directly related to the subject of this work was discovered. We clarify its essence considering the redox processes of copper in a 1 M KOH solution (Figure 3). The experiment was started with fixed parameters controlling the oscillation of specimens (see Equation 2) and contact surfaces, which were completely reduced at $E = -1.2$ V. For potentials below −0.3 V (marked with an arrow),

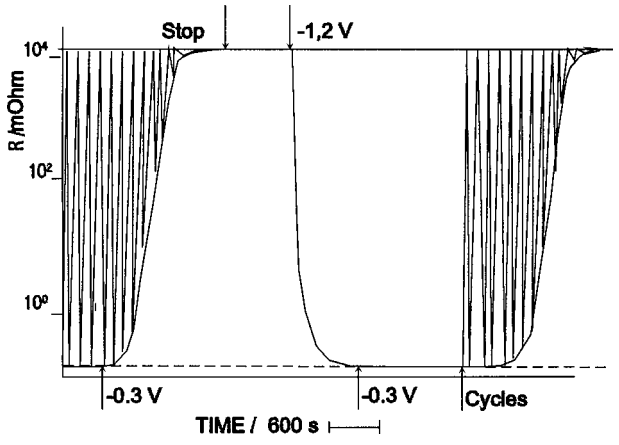

Fig. 3. The copper CER during oxidation and reduction at open and closed contacts. The measurements are started on clean surface at $E = -1.2$ V. At $E = -0.3$ V (marked with an arrow), the oxidation begins. The 'Stop' arrow denotes a stop specimen cycling at the maximum compression with the oxidized contact surfaces. At $E = -1.2$ V (an arrow), the clamped surfaces rapidly reduce. At $E = -0.3$ V (an arrow), the clamped contact surfaces does not oxidize until the cycling is resumed ('Cycle' arrow). See text for details.

the CER of clean copper surfaces was 0.2 mΩ. Once a potential $E = -0.3$ V is set, submonolayer oxide growth begins ($E^0_{Cu_2O} = -0.36$ V), and within 15 min the CER of copper reaches 10 Ω. This means that the whole contact surface of copper is covered with one or two oxide monolayers [10, 11]. Numerous repeated experiments showed that, if E is switched to −1.2 V again, the contact surface quickly reduces and the CER decreases to the original value (not shown in Figure 3). A similar rapid reduction of copper, is achieved if, at $E = -0.3$ V, the mobile electrode is stopped at the moment of the maximum clamping of contact surfaces (shown with a 'Stop' arrow) and then a potential $E = -1.2$ V is applied. If the cyclic motion is not resumed and $E = -0.3$ V is reset again (indicated in Figure 3 by arrow), the clamped contact surfaces do not oxidize for up to a week, but quickly oxidize once cycling is resumed (see the arrow 'Cycles'). Similar results differing only in the oxidation and reduction potentials were obtained for silver, gold, and platinum. The contact surfaces, which were preliminary oxidized and then clamped, quickly reduce without cycling, while the surfaces, which were initially cleaned of films and then clamped, do not oxidize until the cycling is resumed.

When the contact surfaces are compressed together, only the reduction of the earlier formed oxides is possible, while oxidation of clean contact surfaces does not occur. This means that the cathodic polarization of the walls of super narrow gaps is highly effective, while the anodic polarization is completely ineffective. This paradoxical situation cannot be explained in terms of published results [1–6]. However, an explanation is possible if one takes into account the different width and state of a gap between the compressed clean and compressed oxidized contact surfaces. In the former case, the gap is not present, since the polished surfaces are in tight contact with each other. Their roughness is smoothed under the effect of the contact pressure and the electrolyte is insulated within micro volumes located between them and no conductive path to the bulk electrolyte exists. In this case, neither cathodic nor anodic external polarization of the contact surfaces is possible. In the latter case, contact surfaces are covered with *a continuous copper oxide layer with a thickness of 1–3 nm*. At low overvoltages (about 0.05 V), one or two monolayers of oxide with a thickness of 1–3 nm are formed on copper in a 1 M KOH solution in 10–15 min. This is confirmed by the investigation of the kinetics of submonolayer growth of copper and silver oxides [11] and SERS data [12]. Thus, a thin, continuous oxide layer between the electrode surfaces is in contact with the electrolyte in the cell and can be reduced under cathodic polarization, but cannot grow under anodic polarization. The quick and complete reduction of the contact surfaces, which were preliminary oxidized and clamped, can be accounted for by penetration of the electrolyte (and the polarizing external current) into the contact as the oxide layer gradually reduces. Based on this explanation and assuming L equal to the contact

surface radius (1 mm) and $W = 1$–3 nm, we have $L_{cr} = 10^6$–10^5 W, which exceeds the theoretical estimates [1, 2] by 10^4–10^5.

3.2. *A valuation of electrolyte resistivity in submicron gaps*

The above examples of $L_{cr} \gg 15\ W$ suggest that the conductivity of the electrolyte sharply increases in submicron gaps. The validity of this supposition can be studied experimentally with the CER technique modified so that the CER dependence of the clean contact surfaces on the deformation of the mild spring ΔL (at $P_1 = \text{const}$, and $P_0 = f(t)$, see Equation 2) can be recorded. The specimens, which were clamped with some load at the beginning of the experiment, were gradually drawn apart to a certain distance, at which the electric contact was completely lost. Below, we refer to these $R = f(L)$-curves as distance–resistometric (DRM) curves. During the CER measurement, the lower specimen I (insert in Figure 4) is fixed, while the upper one II is moved reciprocally along the common axis with amplitude of 5 μm. If the specimens are not in contact, $\Delta l = 0.001\ \Delta L$. In contact, the deformation of a rigid spring 7 (Figure 2) is restricted by the specimens, which undergo elastic deformation. In this case, $\Delta l < 0.001\ \Delta L$ and depends on the compliance of specimens, which amounts to 0.1 μm kg^{-1}. Figure 4 illustrates how the CER values and the compliance of the rigid spring are related to the tension deformation of the mild spring ΔL. The experiments were carried out with copper specimens in 1.0 M KOH solution at a potential of −1.1 V, at which contact surfaces are free of any films. At the beginning of the experiments, the specimens were clamped together strongly, so that the subsequent elongation of the mild spring (Figure 2) by $\Delta L = 1$, 1.5 and 2 mm could not result in a sharp increase in CER values. Then, ΔL was increased in steps of 0.05–0.25 mm, and CER (curve 1) and compliance C values (curve 2) were measured.

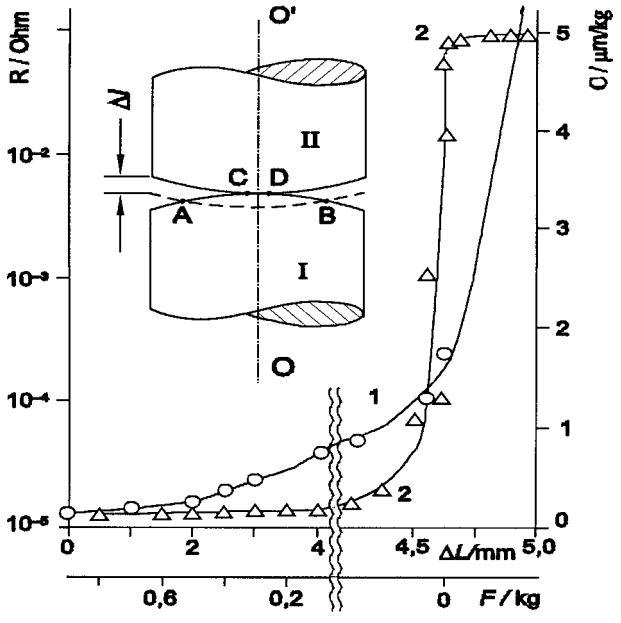

Fig. 4. (1) The CER of copper (R) in a 1 M KOH solution at $E = -1.2$ V and (2) the compliance of the rigid spring C vs the elongation of the mild spring (ΔL) and the contact compression (F). An insert shows the change in the contact surface area at a decrease in the contact compression (see text for details).

Zero ΔL in Figure 4 is chosen arbitrarily, but it corresponds to a hard enough contact between specimens. In the insert, the location of the upper specimen II at $\Delta L = 0$ is shown with a dashed line. At this position, the diameter of the contact surface is equal to AB. An elongation of the mild spring by Δl leads to a shift of the upper specimen by Δl and a decrease in the contact surface to CD. Subsequent elongation further decreases the contact surface and finally results in the complete loss of the mechanical contact between specimens. Treating the contact surface as a circle is conditional [13], but irrespective of the shape of the contact surface, its area decreases with an increase in ΔL and ΔI.

At a strong initial compression, the plastic deformation of the most protruding micro wrinkles of the contact surfaces occurs. This is a period (20–30 min) of aligning of contact surfaces when the CER of clean surfaces slightly decreases and reaches its steady-state value. Then, at a smaller pressure, only the elastic deformation of specimens takes place. As follows from Figure 4, at the beginning of the elongation of the mild spring ($\Delta L \ll$ 4 mm), the CER noticeably increases owing to a decrease in the contact area. The compliance remains equal to 0.10–0.12 μm kg^{-1}, which is typical of the elastic deformation of the specimens. A further increase in ΔL to >4 mm is followed by a sharp increase in the compliance to a value of 5 μm kg^{-1}. At $\Delta L = 4.65$ mm the mechanical contact between the specimens is lost. This defines the zero point of the compression scale F in Figure 4. It is important that to note that the mechanical contact is lost much earlier (curve 2) than the electrical contact (curve 1). In the absence of mechanical contact, the CER is determined by the conductivity of an electrolyte layer with a thickness of 0.4 μm between the contact surfaces of the specimens.

When studying the conductivity of solutions in super narrow gaps, one should compare the DRM curves obtained in various media: in air, in aqueous and nonaqueous solutions. This generates several problems with experimental methodology. First of all, each contact couple is unique, i.e., the DRM curves in different environments should be recorded and compared for the same contact couple. Next, it is highly desirable to obtain a reference DRM curve for this couple in the air for subsequent comparison with the curves recorded in solutions. Below, DRM curves in different environments for each contact couple are given in separate figures.

The original A_0 value (Equation 2) selected for a particular series is controlled at the beginning of each experiment. The ΔL and Δl values corresponding to A_0 are considered as the zero point of the abscissa axis. Such a control of initial experimental conditions pro-

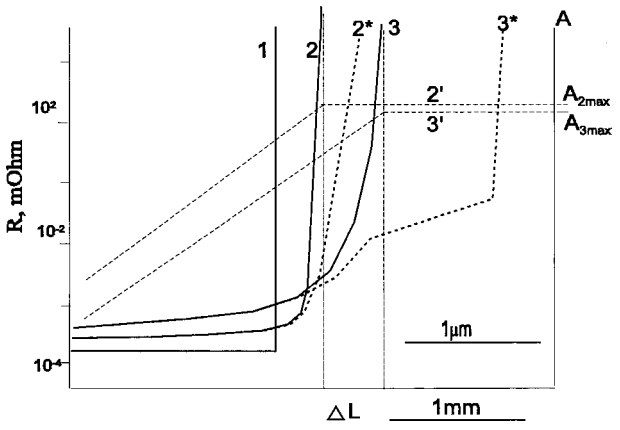

Fig. 5. Schematic distance–resistometric (DRM) curves in air and in an electrolyte: (1) perfectly polished parallel contact surfaces of the metal not deformed and not oxidized in air; (2) mirror-polished gold in air; (3) sandpapered (SiC, grade 1000) gold in air; (2* and 3*) the same gold contacts in an electrolyte; and (2′ and 3′) the oscillation amplitude of specimens in air and in an electrolyte depending on the elongation of the mild spring (ΔL). See text for details.

vides the low enough scattering of DRM curves, e.g., for gold in air, at the complete loss of metallic contact $\Delta l = \text{const} \pm 0.1\ \mu\text{m}$. In air, the CER of freshly polished contact surfaces of nickel, copper, silver and platinum (but not gold) increases from 30–70 $\mu\Omega$ up to 1.0 Ω in 30 min due to oxidation of these metals.

A scheme in Figure 5 gives a general idea of how the DRM curves for gold in air and solution depend on the pretreatment of the contact surfaces. A perfect non oxidized contact would obviously have a DRM curve 1 with no CER increase in the initial range, when the metallic contact exists, but a steep ascent upon separation of contact surfaces by 1–2 nm. DRM curve 2 corresponds to the actual gold contact after the mirror polishing (SiC sandpaper of grade 4000). The first segment of this curve has a small slope that abruptly transforms into a relatively steep ascent of the CER with an increasing slope. A similar form (curve 3) with a larger slope for the initial segment and less steep, but also increasing slope of the CER in the second segment, is typical for contacts polished with SiC paper of grades 800 or 1000. A continuous increase in the CER slope within the second segment reflects the pronounced loss of metallic contact indicating the proper (coaxial) fastening of specimens. Only such 'proper' contacts were studied in this work.

An important characteristic of proper contacts are the clear cat breaks of the amplitude curves 2′ and 3′ in Figure 5 that correspond to the moments when the maximum amplitude of oscillations is reached, i.e., when the metallic contact is completely lost. This is especially important, since the DRM curves of gold in electrolyte solutions so drastically differ from those originally obtained in air (cf. Figures 5 and 6) that it is already

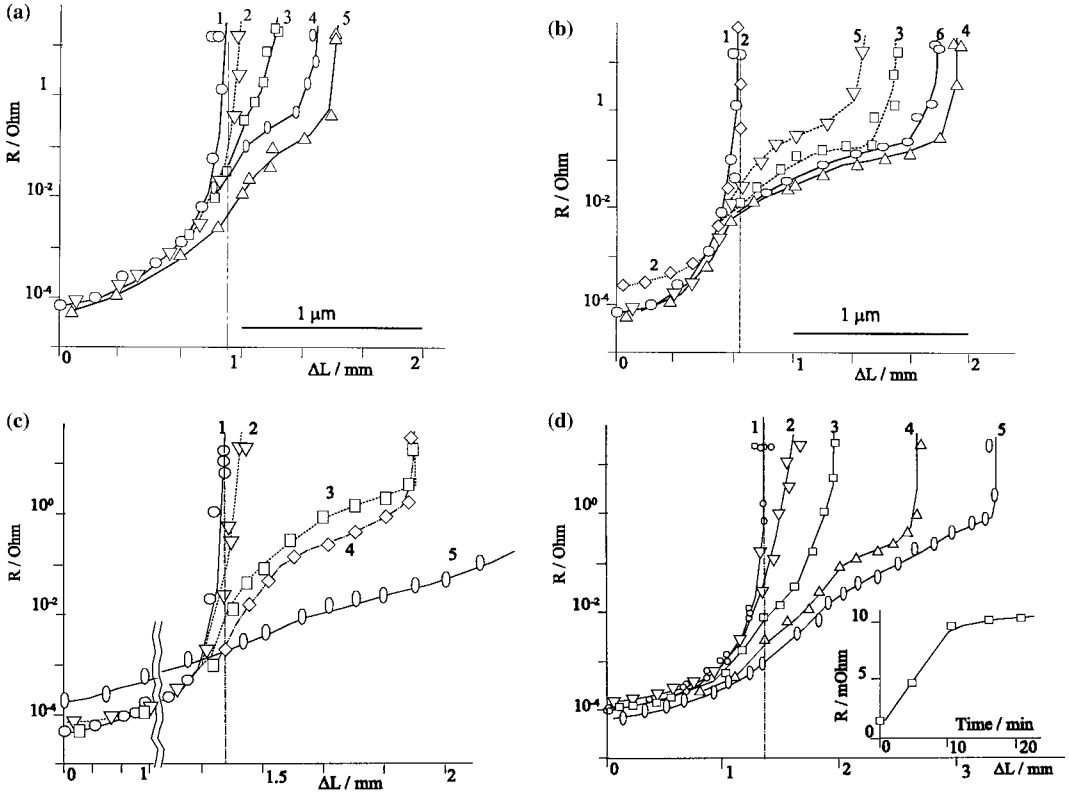

Fig. 6. DRM curves of gold (grounded with SiC, grade 1000) in air and in electrolytes. The numbers of curves denote the order of replacing experimental conditions for each contact couple: (a) (1) air; (2) ethanol + 5 vol % H_2O + 0.02 M NaCl; (3) ethanol + 15 vol % H_2O + 0.02 M NaCl; (4) 4 M HNO_3; (5) H_2O + 0.001 M NaCl; (b) (1) air; (2) 10 M LiCl; (3) 5 M LiCl; (4) H_2O + 0.001 M LiCl; (5) 5 M LiCl; (6) H_2O + 0.001 M LiCl; (c) (1) air; (2) 10 M H_2SO_4; (3) 4 M H_2SO_4; (4) H_2O + 0.02 M NaCl; (5) 4 M KOH at the cathodic polarization with 30 μA; (d) (1) air; (2) 4 M HNO_3; (3) H_2O + 0.001 M NaCl; (4) 1 M KOH at the polarization with 60 μA; (5) 1 M KOH at the polarization with 150 μA. An insert show the kinetics of the CER increase upon replacement of 1 M KOH with 1 M H_2SO_4 at $\Delta L = 1.5$ mm = const.

impossible to observe the moment when the metallic contact is lost leading to an increase in CER. The moment when the maximum amplitude of oscillations is reached, and the moment when a sharp increase in the compliance of the rigid spring occurs, reflect a mechanical characteristic of the contact and are independent of the electrochemical conditions of the experiment. Upon the loss of metallic contact, the increase in the mean distance between contact surfaces $\Delta l = 0.001\ \Delta L$.

In the same electrolyte, e.g., in a 0.1 M HCl solution, with completely cleaned contacts, the DRM curves of mirror-polished (2) and ground (3) gold contacts changes differently. Their initial segments, which reflect chiefly the CER of clean metallic contacts, does not change significantly, while the steeply ascending segments, when metal contacts quickly disappear, become more slanting and extend to the range where the metal contact is absent (curves 2* and 3* and amplitude curves 2′ and 3′ in Figure 5, respectively). On the complete loss of electrical contact, the difference is 0.3–0.4 μm for mirror-polished contacts and 0.7–1 μm for ground contacts. Obviously, the CER value measured upon the loss of metallic contact is determined by the conductivity of a submicron electrolyte layer between contact surfaces drawn apart. As was noted above, the ionic electrical conductivity of solutions cannot be measured under our experimental conditions (direct current at a low, 0.1–1.0 mV, voltage drop). For nonionic conductivity, we note that, as the distance between microcontacts (tip of the scanning tunneling microscope [14], crossed cylindrical [15] or spherical [16] atomically smooth surfaces) in electrolytes was changed, only the electron tunnel currents at distances of up to 1 nm were observed. This distance is three orders of magnitude smaller than the distances dealt with in our work; that is, electron tunneling cannot account for the phenomenon observed in this work. However, we should stress that the contacts studied in works [14–16] are essentially point contacts and do not adequately represent a three-dimensional electrolyte layer in actual super narrow gaps and cracks.

We must consider the possible causes of the difference between DRM curves of the polished 2* and ground 3* contacts in Figure 5. Each contact spot on a mirror-polished surface can be thought of as a contact couple (as shown in Figure 4) that resembles a contact between two spherical surfaces. The density of such spots on the mirror-polished contact surface is small, while the surface area of each spot is relatively large. Therefore, during the alignment of electrodes under heightened compression, these spots are elastically deformed. With a gradual increase in ΔL and the loss of mechanical contact, each spot transforms into a point contact, for which the role of conductivity of an electrolyte layer with a thickness more than 1 nm is insubstantial [14–16]. By contrast, the density of contact spots on ground surfaces is much higher, while the area of each spot is smaller. These spots are sharp, which results in high local compression forces during the alignment of electrodes and the mutual plastic deformation of the most protruding sites. During the alignment of ground contacts, a large number of such contact couples with complementary surfaces are formed. The real contact consists of numerous microcontacts separated with micro cavities filled with an electrolyte. The alignment results in a smoothing of the ground contact. It becomes morphologically similar to a stress corrosion crack, the walls of which are also complementary surfaces far from the mirror state. In air, such a ground contact has a smaller summary area of metallic contacts and a higher CER value than does a mirror-polished contact. In solution, however, a ground contact has a larger area of the thin electrolyte layer, which may decrease the CER at low contact compression forces and after the complete loss of metallic contact (see curves 2 and 3 in Figure 5).

Figure 6 shows DRM curves for gold ground contacts. At the beginning of each run, DRM curves were recorded two to four times in air at a constant initial ΔL value in order to check the quality of the contact. These are the reference curves 1 in Figure 6a–6d. In the Figure, the loss of metallic contact is marked with vertical dashed lines. Then, at the same ΔL values, measurements were carried out in (a) alcohol, (b) salt, (c) acidic, and (d) alkaline solutions. The numbers of curves in Figure 6a–6d reflect not only the composition of a solution, in which each DRM curve was recorded, but also the order of measurement in the various solutions. This allows one to judge the reproducibility of the results obtained in two solutions with their repeated replacement. For instance, when comparing curves 3 and 4 in Figure 6b, we can see that the conductivity of a concentrated LiCl solution is lower than that of a dilute solution. This contradicts to the expected concentration dependence of the ionic conductivity of aqueous electrolyte solutions. However, the repeated replacement of the solutions for the original contact couple provided the same result, despite a certain shift of curves 5 and 6 with respect to curves 3 and 4.

While each contact couple is unique, repeatedly recording DRM curves for various contact couples at various initial contact pressures and with various orders for solution replacement enabled us to obtain a correct picture of the relative conductivities of the studied solutions in submicron gaps. Each of Figure 6a–6d shows not only the DRM curves for a particular contact couple, but also their position with respect to the reference curves of other specimens. This experimental series shows that the nature of the electrolyte dissolved in water–alcohol mixtures at a concentration of 0.01 M is insubstantial. The position of the DRM curves is determined by water content: for $[H_2O] \leqslant 10$ vol %, the DRM curves 2 are very close to the reference curves 1 or coincide with them; for $[H_2O] = 15$ vol %, the curves 3 already noticeably deviate from reference curves 1; and for $[H_2O] \geqslant 50$ vol %, the DRM curves 5 are practically independent of ethanol content and deviate substantially from the reference curves 1. The

DRM curves 4 in strong nitric acid lies typically to the left of curves 5 (see also Figure 6c and d).

As follows from Figure 6b and c, the higher the concentration of electrolyte dissolved in water, the smaller the contribution of the solution to the conductivity. For example, the DRM curves 2 in 10-M aqueous LiCl or H_2SO_4 solutions are close to the reference curves 1. The conductivity of strong LiCl solutions (curves 3 and 5) is close to and even smaller than the conductivity of a 0.001 M solution (curves 4 and 6 in Figure 6b). The same occurs in the case of sodium and potassium chlorides, as well as in nitric (Figure 6a and d) and sulfuric (curves 3 and 4 in Figure 6c) acids. This latter fact is worth special note, because 4-M solutions of these acids have a specific conductivity close to the maximum value (0.75 Ω^{-1} cm^{-1}).

Curve 5 in Figure 6c convincingly shows that the above trend of a decrease in the electrical conductivity of strong and concentrated salts and acids solutions compared to dilute solutions in submicron gaps is not typical of alkaline solutions. Despite a noticeable increase in the CER of gold in a 4 M KOH solution at high contact pressures caused by the adsorption of hydroxide ions [10, 11], curve 5 after the loss of mechanical contact lies substantially below the other DRM curves, including curve 4 recorded in a dilute solution. The detailed DRM curves for gold in a 1 M KOH solution are given in Figure 6d, which shows that the conductivity of the alkaline solution increases with a decrease in the potential. A special series of experiments demonstrated that the conductivity of all studied 1 M alkaline (LiOH, NaOH, KOH, and CsOH) solutions in submicron gaps is higher than that of weak and strong solutions of acids and salts.

If, after recording the DRM curve 5 in Figure 6d, the alkaline solution is replaced with a 1 M H_2SO_4 solution, the resulting DRM curve is close to curve 3 (not shown in Figure 6). The insert in Figure 6d shows the kinetics of the CER increase after such a solution replacement at constant $\Delta L = 1.5$ mm. This increase reflects the exchange between the initial alkaline solution and the new acidic solution. An additional series of experiments showed that the repeated replacement of a 1 M alkaline solution, after recording a the DRM curve, with a 1 M acidic solution and *vice versa* leads to the same result: upon the loss of metallic contact, the CER in alkaline solutions is lower than that in the acidic solution by a factor of 5–10, although the ionic electrical conductivity of equinormal acidic solutions is typically higher than that of alkaline solutions by a factor of 2.5. Moreover, the complete loss of contact in alkaline solutions requires that the contact surfaces be drawn apart to a much larger distance than in acidic solutions (by 0.5–1 μm). Thus, alkaline solutions in submicron gaps have an especially high conductivity. This may partly explain the heightened electrical conductivity of the diluted solutions (see above). Indeed, for cleaning contact surfaces, CER measurements were carried out under cathodic polarization, which may transform the originally neutral or weakly acidic solution in the gap between electrodes into an alkaline one.

3.3. *Model of anomalous conductivity in submicron gaps*

The results obtained show that, during CER measurements, with a gradual increase in the distance between the contacts, a 0.5–2 μm thick electrolyte layer with an anomalously low resistivity, ρ, exists between them. Try to estimate ρ for alkaline solutions from the relative positions of curves 1 and 5 in Figure 6c and 6d. Upon the loss of metallic contact, the CER is about 0.001 Ω (see the intersections of curves 5 with the vertical dashed lines). Assuming an apparent contact area of about 10^{-4}–10^{-2} cm^2 and a mean distance between the contacts of around 10^{-5} cm, we come to $\rho = 0.01$–1 Ω cm. An intermediate ρ value is 0.1–10 Ω cm (at a mean distance between contact surfaces of 1.5×10^{-4} cm and a CER value of 10^{-2} Ω), while just before the complete loss of electric contact at a CER = 1 Ω, $\rho = 0.5$–50 Ω cm. Note that ρ values are not constant and sharply as the electrolyte layer thickens.

The low value obtained (0.01 Ω cm) is a characteristic of semiconductors rather than solutions. This fact, along with the aforementioned unusual ratios for the electrical conductivities of dilute and strong solutions cannot be explained in terms of the standard concept for the ionic conductivity of solutions, including the proton exchange mechanism of Grotthus [17–20]. The same can be said about the shape of the DRM curves in Figures 5 and 6, consisting of two segments: at first at initially slow increase in CER, followed by a much more rapid increase would be impossible if the electrical conductivity were independent of the distance of separation. These observations suggest there must be some particular property of aqueous solutions, which is most pronounced at the metal–solution boundary and quickly weakens with the distance from the boundary. Such a property could be a spatial hydrogen-bonded network (HBN) possessing an ice-like structure close to the metal surface [17–33]. This supposition is based on the following data:

1. a high electrical conductivity is obtained for ice at a sufficiently high concentration of charge carriers [17–20]. A similar situation could exist in liquid provided that there is a sufficiently widely branched and relatively ordered bonded network of similar molecules involving hydroxyl groups and characterized by short-range interactions;
2. high conductivities of solvents with a HBN [21–26] to which water, but not alcohols, belong. Such a bonded network is labile, stable against external effects, and able to transmit perturbations over the whole volume [21–23]; and
3. a similar network can exist in the ordered layered structure of water adsorbed on nonmetals, silver, gold, and platinum [14, 30–32]. Such an the ice-like structure of water on mercury [16] has been predicted theoretically in molecular dynamics simula-

tions and discovered experimentally by several independent *in situ* techniques [29–32].

The estimated thickness of such an ordered boundary layer of adsorbed water varies from several nanometers to microns [30]. However, most experimental works indicate that this layer is about 1–1.2 nm, i.e., involves four to five molecular layers of water [16, 30–32]. It is worth noting that these layers are stable and exist long enough that their in-layer density can be determined by X-ray spectroscopy [31], and the structural modification of ice (Ih) can be determined with the tunnel current [16]. In both cases, the most intense signals were obtained from the first monolayer of adsorbed water, while the second, third, and fourth layers gave successively decreasing signals. The signal from the fifth layer was indistinguishable. It is quite probable that the fifth and subsequent ordered layers of water do exist, but their high lability does not allow their experimental detection.

Super fast proton transfer in ice is related to the cooperative charge transfer and orientation of Bjerrum's defects, a process much more efficient than Grotthus's mechanism [19, 20]. This cooperative mechanism in water should be still more effective; however, it will not work until the spatial HBN forms. For instance, in solid highwater hydrates of heteropolyacids, the electrical conductivity reaches 0.17 Ω^{-1} cm^{-1} [20]. There is 'protonic superconductivity' in numerous biological systems that have a capillary structure, in which adsorbed water has an ordered structure [19]. As we know, such a possibility has not been considered in the case of metals, although, in this respect, there is no principal difference between biological and metallic capillaries, and the structure of water adsorbed on the latter is also likely to be ordered due to the HBN formation [16, 28, 31].

The above facts and ideas suggest the following model for electrical conductivity of aqueous solutions in submicron gaps. Water layers adsorbed on contact surfaces have an ice-like structure stabilized with hydrogen bonds. As the distance from the metal increases, these layers become more and more labile. In the bulk solution between contact surfaces, there are clustered fragments of the spatial HBN [21–24], which can reorient and align to the spatial structures existing near each contact surface. The degree of such reorientation may depend on the electric field intensity between the electrodes. Thus, a labile structure of water molecules forms. Its thickness may substantially exceed the thickness of the two double layers associated with the individual contact surfaces. The electrical conductivity of such a structure will be close to the conductivity of ice until the time of charge transfer (about 10^{-14}–10^{-15} s [17]) is noticeably smaller than the lifetime of the spatial HBN. Consider some consequences that can be derived from this model and its correlation with the experimental data.

1. In ethanol solutions, hydrogen-bonded chains for prototronic charge transfer may form [18], but cannot be joined in a spatial HBN [21]. According to the model proposed, the CER of gold in pure alcohol should be determined primarily by the metallic contact, as observed experimentally (Figure 6a).
2. The electrical conductivity of the solution layer between the contact surfaces should primarily depend on the quality and extension of the spatial HBN rather than on the nature and concentration of dissolved electrolytes. Thus, the ionic conductivity of the solution should not play a decisive role, as observed experimentally.
3. A high electrolyte concentration may decrease the probability of formation, and hence the conductivity of an HBN, since a substantial part of water molecules will be engaged in the maintenance of solvation shells around the ions, loses their mobility and cannot effectively participate in the formation of a spatial HBN. This is confirmed by the data in Figure 6b–d and the results [34, 35]. Using the technique of differential thermal analysis, the authors [35] showed that there is no free water in LiCl solutions at concentrations above 9.13 M. Typical hydrogen ion hydrates include $H_5O_2^+$, $H_7O_3^+$, and recently discovered $H_9O_4^+$ [34]. This means there is practically no free water, which could be involved in the formation of a spatial HBN, in 10 M sulfuric acid solutions. In fact, the electrical conductivity of gold contacts in 10 M lithium chloride and sulfuric acid solutions is determined by the metal alone as in ethanol.

3.4. *External electric field effect*

The appearance and stabilization of a labile HBN can be promoted by the formation of several structured layers of adsorbed water near each contact surface and the existence of a potential difference between the electrodes. To check this hypothesis, we carried out special experiments on gold where the potential difference between electrodes ΔE was varied from 10^{-6}–2×10^{-2} V. Preliminary results indicate that changes in ΔE within these limits do not affect the DRM curves of gold in air.

In order to quantitatively treat the results, a deviation (Δl) of each DRM curve measured in solution from the reference curve in air was estimated. The data obtained are shown in Figure 7. Despite a substantial scattering, one can see that the anomalously high conductivity of aqueous solutions in submicron gaps appears at $\Delta E \geqslant 10^{-5}$ V and increases with an increase in ΔE up to 10^{-3} V. This range corresponds to the electric field intensity $\Delta E/\Delta l$ of 1–10 V cm^{-1}. These data do not contradict the supposition on the relation between the formation of a labile spatial HBN in submicron gaps and the potential difference between contact surfaces and show that, at $\Delta E/\Delta l \leqslant 1$ V cm^{-1}, this network spreads to a distance no larger than 10^{-5} cm from each contact surface.

Quantum mechanical simulations [36, 37] showed that, as the electric field intensity is increased to

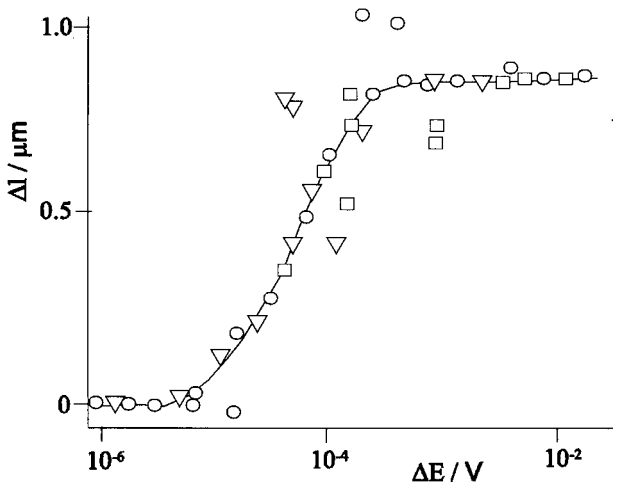

Fig. 7. Deviations (Δl) of the DRM curves of gold in 0.01 M (◯) KOH, (▽) KCl, (⊕) HCl, and (□) H_2SO_4 solutions from the DRM curves recorded in air vs. the potential difference between the specimens.

10^7–10^8 V cm^{-1}, a phase transition of the order–disorder kind takes place, an ice-like water structure is formed, and the proton-transfer energy barrier is decreased or even levels off. Such local field fluctuations can easily appear in aqueous solutions at room temperature [37]. The role of the metal - solution boundaries, which can promote the formation of HBN, was not considered.

An accelerating effect of electric fields with an intensity of 10^{-3}–10^{-1} V cm^{-1} was experimentally discovered during the growth of some biological systems in water [38]. It is worth noting that biological processes proceed typically in submicron cavities separated with the cell walls and membranes where boundary surfaces play a very important role [19, 38]. Probably, for this reason, the field intensity determined in [38] is noticeably closer to the data of our work than to calculated data [36, 37]. There are experimental results [39, 40], by which the field intensity sufficient for an accelerated proton transfer and a water dipole reorientation, is 10–100 V cm^{-1}, which is also closer to our data than to results [36, 37].

Conclusions

1. A 0.5–2 μm thick aqueous solution layer between macro contacts was found to have a high enough conductivity of nonionic nature. This is confirmed by data on SCC of high-strength steels and on the CER measurements.
2. Model has been proposed, by which the high electrical conductivity of aqueous solutions in submicron gaps is determined by the charge transfer along the spatial hydrogen-bond network that forms under the effect of a potential drop between contact surfaces. This model consistently accounts for experimental results.
3. Concentrated aqueous solutions of salts and acids are shown to have lower electrical conductivity in narrow gaps as compared to dilute solutions. This is related to the hydration of ions and the corresponding decrease in the free water content able to participate in the hydrogen-bond network.
4. The heightened electrical conductivity of alkaline solutions in submicron gaps is typical for all the studied electrodes in alkalis at a concentration of above 1 M.
5. The anomalously high conductivity of aqueous solutions in submicron gaps was shown to depend on the voltage drop between contact surfaces ΔE. It appears at $\Delta E \geqslant 10^{-5}$ V and increases with an increase in ΔE up to 10^{-3} V.

Acknowledgements

Author thanks Professor David Shoesmith (University of Western Ontario, Canada) for useful comment on a draft version of the manuscript. Experiments were carried out in Institute of Physical Chemistry of Russian Academy of Sciences. Russian Foundation for Basic Research has supported this work, project number 01 03 32012.

References

1. A.N. Frumkin, *J. Phys. Chem. (USSR)* **23** (1949) 1477 (in Russian).
2. E.M. Gutman, 'Mechanochemistry of Metals and Corrosion Protection' (Metallurgiya, Moscow, 1974) (in Russian).
3. A. Turnbull and M. Psaila-Dombrowski, *Corros. Sci.* **33** (1992) 1925.
4. A. Turnbull, *Corros. Sci.* **39** (1997) 789.
5. B.G. Ateya and H.W. Pickering, *Corros. Sci.* **37** (1995) 1443.
6. D.T. Chin and G.M. Sabde, *Corrosion* **55** (1999) 229.
7. V.A. Marichev, *Prot. Met.* **16** (1980) 531 (in Russian).
8. V.A. Marichev, V.A., *Usp. Khim.* **56** (1987) 732 (in Russian).
9. V.A. Marichev, *Werkst. Korros.* **33** (1982) 1; **40** (1989) 304.
10. V.A. Marichev, *Russ. J. Elecktrochem.* **35** (1999) 456.
11. V.A. Marichev, *Surf. Sci. Rep.* **44** 3/6 (2001) 51.
12. H.Y.H. Chan, C.G.Takoudis and M.J. Weaver, *J. Phys. Chem. B.* **103** (1999) 357.
13. R. Holm, 'Electric Contacts Handbook' (Springer, Berlin 1958).
14. G. Nagy, *Electrochim. Acta* **40** (1995) 1417.
15. F.-R.F. Fan and A.J. Bard, *J. Amer. Chem. Soc.* **109** (1987) 6262.
16. J.D. Porter and A.S. Zinn, *J. Phys. Chem.* **97** (1993) 1190.
17. E. Gruwald, in: S.G. Cohen, A. Streitwieser and R.W. Taft (Eds.), 'Progress in Physical Organic Chemistry', Vol. 3. (Wiley, New York, 1965).
18. T. Erdey-Gruz, in 'Transport Phenomena in Aqueous Solutions', (Academiai Kiado, Budapest, 1974).
19. V.Ya. Antonenko, A.S. Davydov, A.S. and V.V. Il'in, 'Basic Principles of Water Physics', (Naukova Dumka, Kiiv, 1991) (in Russian).
20. A.B. Yaroslavtsev, *Usp. Khim.* **63** (1994) 449 (in Russian).
21. M.N. Rodnikova, *Russ. J. Phys. Chem.* **67** (1993) 275 (in Russian).
22. M.N. Rodnikova, *Doctoral (Chem.) Dissertation*, Inst. General and Inorg. Chem., (Moscow 1998 (in Russian).
23. N.A. Chumaevskii, A.G. Novikov and M.N. Rodnikova et al. *Inform. Bull. RFFI*, **5** (1997) 303.

24. A.K. Lyashchenko, Russian *J. Phys. Chem.* **67** (1993) 281(in Russian).
25. N.A. Bul'enkov, *Kristallographiya* **33** (1988) 424 (in Russian).
26. M. Szafran, *J. Mol. Struct.* **381** (1996) 39.
27. A.M. Brodsky, M. Watanabe and W.P. Reinhardt, *Electrochim. Acta* **36** (1991) 1695.
28. A. Calhoun and G.A. Voth, *J. Phys. Chem. B* **100** (1996) 10746.
29. G. Nagu and G. Denuault, *J. Electroanal. Chem.* **450** (1998) 159.
30. L. Israelachvili and H. Wennerstrom, *Monthly Nat.* **4** (1996) 62.
31. M.F. Toney, H.J. Howard and J. Richer et al. *Nature*, **368** (1994) 444.
32. A.E. Russel, A.S. Lin and W.E. O'Grady, *J. Chem. Soc., Faraday Trans.* **89** (1993) 195.
33. G. Zilberman, V. Tsionsky and E. Gileady, *Electrochim. Acta* **45** (2000) 3473.
34. N. Chen, P. Blowers and R.I. Masal, *Surf. Sci.* **419** (1999) 150.
35. T. Kawai, Y.M. Lee, K. Nakajima and K. Ehara, *J. Electroanal. Chem.* **422** (1997) 133.
36. G. Sutmann, *J. Electroanal. Chem.* **450** (1998) 289.
37. K. Hermansson and L. Ojamae, *Solid State Ionics* **77** (1995) 34.
38. H.-G. Stenz, B. Wohlwend and M.H. Weisenseel, *Bioelectrochemistry* **44** (1998) 261.
39. D.V. Tichomilov, O.N. Slyadneva, *Int. J. Multiphase Flow* **26** (2000) 1891.
40. S. Mafe, P. Ramirez and A. Alcaraz, *Chem. Phys. Lett.* **294** (1998) 406.
41. G. Gabetta and E. Garetta, in: A. Turnbull (Ed.), 'Corrosion Chemistry within Pits, Crevices, and Cracks, (HMSO, London 1984).
42. V.V. Panasyuk, L.V. Ratych and I.N. Dmytrakh, *Sov. Mater. Sci.* **18**(3) (1992) 43; **19**(4) (1983) 33.